6120 *Macromolecules* **2010**, *43*, 6120–6126
DOI: 10.1021/ma100290v

Macromolecules
ARTICLE

# Transition Behavior of Hydrogen-Bonding-Mediated Block Copolymer Mixtures

**Sudhakar Naidu,[†] Hyungju Ahn,[†] Hoyeon Lee,[†] Young Mee Jung,[‡] and Du Yeol Ryu*,[†]**

[†]*Department of Chemical and Biomolecular Engineering, Yonsei University, Seoul 120-749, Korea, and* [‡]*Department of Chemistry, Kangwon National University, Chunchon 200-701, Korea*

*Received February 5, 2010; Revised Manuscript Received April 28, 2010*

ABSTRACT: We have investigated transition behavior for block copolymer (BCP) mixtures composed of a lamella-forming polystyrene-*block*-poly(2-vinylpyridine) (PS-*b*-P2VP) and phenylacetamide derivatives, where the hydroxyl functionality at phenylacetamide unit is available only for 4-hydroxyphenylacetamide (HPA) and not for phenylacetamide (PA). Unlike a similar transition temperature for BCP mixtures with PA, measured by *in situ* small-angle X-ray scattering (SAXS) and depolarized light scattering (DPLS), an annealing temperature dependence for BCP mixtures with HPA indicates that only the complex by H-bonding mediation between the nitrogen units of P2VP block and hydroxyl group in the HPA enhances nonfavorable segmental interactions between two block components, leading to a significant increase in *d*-spacing for BCP mixtures with HPA. This result illustrates the importance of the availability for H-bonding mediation to control over transition behavior for BCP mixtures with the functional molecules.

## Introduction

Block copolymer (BCP) self-assembly, consisting of chemically different polymers linked covalently together, has recently been the focus of active investigations due to the potential necessity of nanoscopic arrays or patterns in applications as the storage media and biomaterials such as data storage, drug release, biodegradable hydrogels, and biomedical applications.[1−7] Such an ability to microphase-separate into mesophases can be attributed to the nonfavorable interactions between two block components, the so-called Flory interaction parameter ($\chi$). When $\chi N$ is sufficiently large ($\chi N > 10.5$ in the case of symmetric BCP) where $N$ is the total number of segments in the BCP, in principle, the microphase separation occurs in tens of nanometers depending on the volume fraction of each component, thereby demonstrating a rich library of mesophases: lamellar (LAM), hexagonally packed cylindrical (HEX), body-centered cubic spherical (BCC), and the complex phase such as gyroid (GYR)[8−14] and hexagonally perforated layers (HPL) which has been believed to be a metastable phase.[14−16] As temperature increases, a phase-mixed (disordered) state can be observed in the weak-segregation regime since $\chi$ is inversely proportional to temperature ($\chi$ decreases with increasing temperature), while microphase-separating upon cooling.[17−19] This phase transition from the ordered to the disordered state occurs at a thermodynamically balanced temperature of $T_{ODT}$, when the nonfavorable interactions are sufficiently weakened and the entropy of mixing in two block components dominates, which is rheologically characterized by a solidlike to liquidlike behavior.[20,21]

In contrast, the supramolecular structures are composed of the specific molecules by use of noncovalent interactions such as hydrogen bonding, leading to the self-organized assembly.[22−40] These supramolecular approaches based on the molecular interactions or complexation can be applied to the polymer systems attractable with a low molecule, as a versatile concept for the preparation of nanostructured and hierarchically assembled macromolecular materials. When one block component of BCP is tuned by the specific interactions such as hydrogen bonding,[22−28] metal coordination,[32−34] and electrostatic interactions,[37−40] the BCP complex may phase-separate into the nanostructures with the built-in assembly, where the small molecule in turn forms the internal interactions within the selective microdomains. Moreover, this simple approach offers advantages over the covalently linked analogues, since the different functionalities can be incorporated into the assemblies simply by substituting the small molecules with the ease of detaching them.[26,36] Several studies have reported that the small molecule into polymers influences the phase transitions depending on the specific interactions with small molecules, as temperature also plays a key role in controlling the strength of the molecular interactions.[27−29]

In this study, we report on the transition behavior for BCP mixtures composed of a lamellar-forming polystyrene-*block*-poly(2-vinylpyridine) (PS-*b*-P2VP) and low molecules depending on hydroxyl functionality at phenylacetamide unit to figure out the influence of the molecular interactions by hydrogen bonding; a 4-hydroxyphenylacetamide (HPA) where two functionalities of hydroxyl and amide units are available and a phenylacetamide (HPA) where one functionality of amide units is available. The transition temperatures, measured by *in situ* small-angle X-ray scattering (SAXS) and depolarized light scattering (DPLS), indicate that the effective hydrogen bonding between BCP and low molecules enhances nonfavorable segmental interactions between two block components during heating process and increases *d*-spacing for BCP mixtures.

## Experimental Section

A BCP, PS-*b*-P2VP, was synthesized by the sequential, anionic polymerization of styrene and 2-vinylpyridine in tetrahydrofuran (THF) at −78 °C under purified argon environment using *sec*-butyllithium as an initiator. Refluxed THF from basic silica column was stirred over fresh sodium−benzophenone complex until it showed a deep purple color, indicating an oxygen- and moisture-free solvent. Degassed monomers with $CaH_2$, styrene, and 2-vinylpyridine (Aldrich) were vacuum-distilled over dried

*To whom correspondence should be addressed: e-mail dyryu@yonsei.ac.kr.

 Published on Web 06/08/2010 

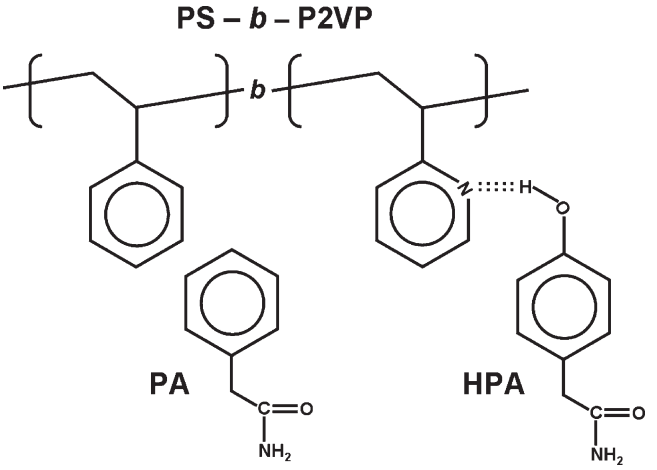


**Figure 1.** Molecular structures for PS-*b*-P2VP, HPA, and PA. A complex formation is indicated by the H-bonding between the nitrogen units of P2VP block and hydroxyl group in the HPA.

dibutylmagnesium and trioctylaluminum, respectively, until a persistent characteristic color was observed. The polymer solution terminated with purified 2-propanol was precipitated in excess hexane. The number-average molecular weight ($M_n$) and polydispersity ($M_w/M_n$) characterized by size-exclusion chromatography (SEC) were 15100 and 1.05, respectively. PS volume fraction ($f_{PS}$) of PS-*b*-P2VP was determined to be 0.504 by $^1$H nuclear magnetic resonance ($^1$H NMR) with mass densities of two components (1.05 and 1.14 g/cm$^2$ for PS and P2VP, respectively). 4-Hydroxyphenylacetamide (HPA; TCI product) and phenylacetamide (PA; TCI product) were used without further purification. The melting temperatures of HPA and PA are 178 and 156 °C, respectively.

BCP mixtures with various amounts of HPA (or PA) were prepared by the freeze-drying method in benzene solutions. For instance, a predetermined amount of PS-*b*-P2VP and HPA is dissolved separately in benzene and ethanol, respectively, maintaining the composition of benzene/ethanol (approximately 1:7 ratio). The concentration of the solution was set to lower than 3% to ensure the homogeneous mixture formation. The quenched solution was evaporated under vacuum for 24 h at room temperature, followed by sequential annealing at 150 °C for 40 h to attain the thermal equilibrium at solvent-free state. The molar ratio of HPA to 2-vinylpyridine units of the PS-*b*-P2VP, denoted to as $x$ = [HPA]/[2VP], was varied up to ~0.10. Especially for BCP mixtures with PA, an annealing temperature was set to 140 °C below the melting temperatures of PA. No macrophase separation was observed for BCP mixtures, which was confirmed by turbidity measurement.

FT-IR spectroscopy (Bruker Tensor 37, Germany) were used to measure the molecular interactions for BCP mixtures with HPA (or PA) at room temperature. All the spectra were collected in a standard wavenumber scan range of 4000 to 600 cm$^{-1}$, the scan number of 64, and the spectral resolution of 4 cm$^{-1}$. The dried samples were physically mixed with potassium bromide (KBr) and pressed to a disk before measurements.

Synchrotron *in situ* small-angle X-ray scattering (SAXS) was used to evaluate the transition temperatures for BCP mixtures, which were performed in 4C1 beamline at the Pohang Light Source (PLS), Korea. The operating conditions were set to a wavelength of 1.608 Å ($\Delta\lambda/\lambda = 1.5 \times 10^{-2}$), the sample-to-detector distance of 2 m, the beam size of 1 × 1 mm$^2$, and the sample thickness of 1.5 mm. A 2D-CCD detector (Princeton Instruments Ins., SCX-TE/CCD-1242) was used to collect the scattered X-rays. The scattering profiles were collected during temperature sweep experiment with the exposure time of ~120 s. Furthermore, depolarized light scattering (DPLS) was used to confirm the transition temperatures using a polarized beam from a He−Ne laser at a wavelength of 632.8 nm, where the intensity detected at photodiode through A/D converter was recorded as a function of temperature. All the heating processes were controlled automatically by a PID controller at constant heating rate of 0.9 °C/min from 140 to 260 °C under the nitrogen flow to avoid thermal degradation of the polymer samples.

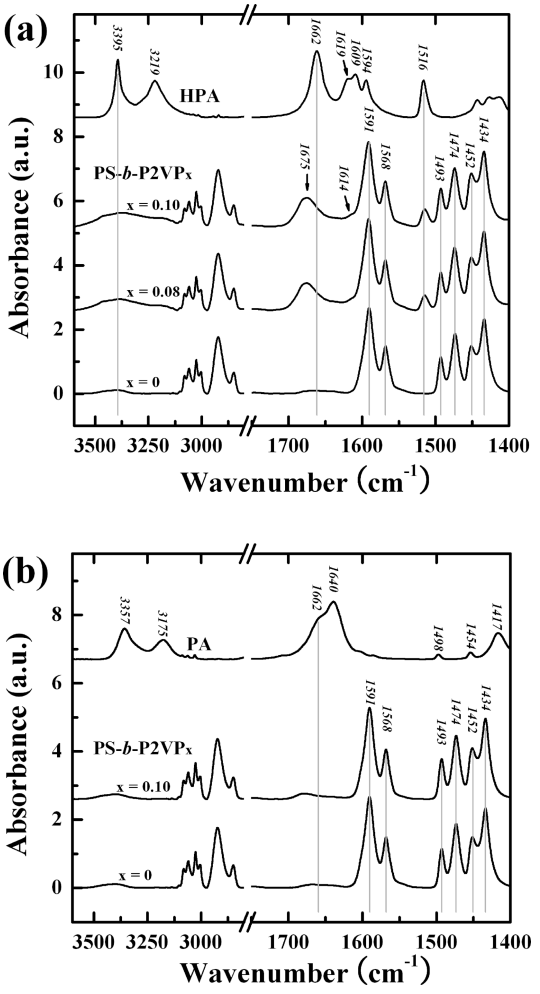


**Figure 2.** FT-IR absorbance spectra for BCP mixtures with (a) HPA and (b) PA. All the spectra were measured at room temperature.

## Results and Discussion

An earlier study by the Brinke and Ikkala group reported that the aromatic alcohols can form hydrogen bonding (H-bonding) with the pyridine units of poly(2-vinylpyridine) (P2VP) and poly(4-vinylpyridine) (P4VP) because they are relatively acidic than alkyl alcohols in terms of proton donation.[35] On the basis of H-bonding capability in the aromatic alcohols, herein, we set the BCP mixtures composed of PS-*b*-P2VP and 4-hydroxyphenylacetamide (HPA) in comparison to those composed of PS-*b*-P2VP and phenylacetamide (PA), as illustrated in Figure 1. HPA involving two functional groups in *para*-positions to the benzene ring is thermally stable due to the intermolecular H-bondings at hydroxyl and methylamide groups and selectively attractable to the nitrogen units of P2VP block via H-bonding at partially acidic alcohol groups, whereas for PA involving only amide group, no hydroxyl group is available.

Figure 2 shows FT-IR absorbance spectra for the pristine PS-*b*-P2VP and BCP mixtures at selected wavenumber ($\nu$) range from 3600 to 1400 cm$^{-1}$ to ensure whether the specific interactions in molecular level are concerned between the units in PS-*b*-P2VP and small molecules. The FT-IR absorbance spectrum for

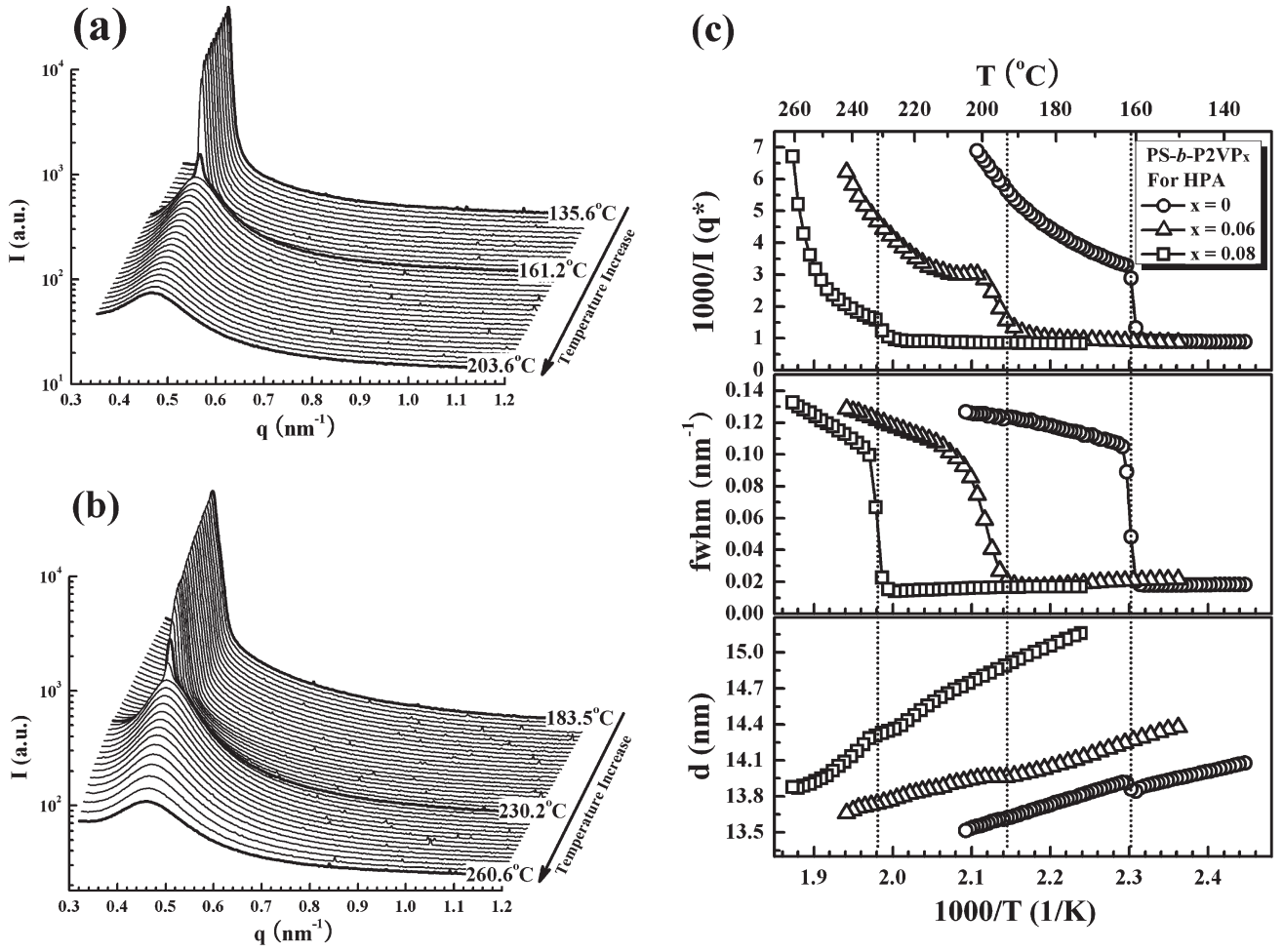


**Figure 3.** SAXS intensity profiles for (a) the pristine PS-*b*-P2VP and (b) BCP mixture with HPA of $x = 0.08$ as a function of scattering vector ($q$) and (c) the scattering parameters derived from the SAXS profiles as a function of inverse temperature (1/K). All the BCP mixtures with HPA were annealed at 150 °C for 40 h before measurements.

the pristine PS-*b*-P2VP and BCP mixtures in Figure 2a,b shows the typical bands due to phenyl ring stretching at 1600 (tiny shoulder), 1568, 1493, and 1452 cm$^{-1}$ and pyridine ring stretching at 1591, 1474, and 1434 cm$^{-1}$, respectively. For the BCP mixtures with a small amount ($x = 0.08$ and 0.10) of HPA in Figure 2a, two bands at 1675 and 1516 cm$^{-1}$ correspond to C=O stretching (amide I band) and aromatic N−H deformation (amide II band with minor contribution of C−N stretching), respectively, indicating a concentration of HPA. A band shift of C=O stretching from 1662 to 1675 cm$^{-1}$ presumably indicates a free C=O from the neighboring H−N in the amide groups due to the low concentration of HPA because the corresponding band at 1662 cm$^{-1}$ for HPA arises from the strong H-bonding environment between two amide groups. With increasing amount of HPA up to $x = 0.10$, a broad band near 3395 cm$^{-1}$, the constant bands for pyridine ring stretching, and a small shoulder band at 1614 cm$^{-1}$ can be attributed to a mild H-bonding between the nitrogen units of P2VP block and hydroxyl group in the HPA, not to the strong protonation of nitrogen. The evidence for a shoulder band at 1614 cm$^{-1}$ was confirmed for BCP mixtures with a large amount ($x \sim 0.4$) of HPA.

For comparison, FT-IR absorbance spectra for BCP mixture with an amount ($x = 0.10$) of PA are shown in Figure 2b. There is neither a broad band near 3357 cm$^{-1}$ nor a characteristic amide band, even though BCP mixture with HPA ($x = 0.10$) shows the characteristic amide I and II bands. These results represent that for the BCP mixtures with HPA the significant amide bands at 1675 and 1516 cm$^{-1}$ are presumably attributed to the influence of the plausible H-bonding between the nitrogen units of P2VP block and hydroxyl group in the HPA, as will be discussed later.

SAXS intensity profiles and the scattering parameters for BCP mixtures with HPA after thermal annealing at 150 °C for 40 h, measured at various temperatures from 135 to 260 °C during heating at a heating rate of 0.9 °C/min, are shown in Figure 3, where scattering vector $q = (4\pi/\lambda) \sin \theta$, where $2\theta$ and $\lambda$ are the scattering angle and wavelength, respectively. As for the pristine PS-*b*-P2VP in Figure 3a, a strong and sharp scattering peak located at $q = 0.446$ nm$^{-1}$ at low temperatures ($T < 160$ °C) arises from the microphase separation due to the nonfavorable segmental interactions between two block components. No second-order peak relative to the first-order reflection (or $q^*$) is caused presumably by the volumetric symmetry between two block components, rather than the low contrast in electron densities between two components is relatively low. Taking it into account that the PS-*b*-P2VP in this study is symmetrically composed of PS and P2VP ($f_{PS} = 0.504$), the morphology should correspond to lamellar microdomains, which is further confirmed to be the same lamellar morphology for BCP mixtures with HPA up to $x = 0.10$ by the peak ratios of $q/q^* = 1{:}2{:}3$ (shown in Figure 8). With increasing temperature for $T > 163$ °C, the primary peak weakens and broadens significantly and then remains to be a diffuse maximum, characteristic of the correlation hole scattering of a phase-mixed (or disordered) BCP. It describes a transition from the ordered to disordered state with temperature, hereafter denoted to $T_{ODT}$ for BCP mixtures. Figure 3b demonstrates SAXS intensity profiles for the BCP mixture with HPA of $x = 0.08$,

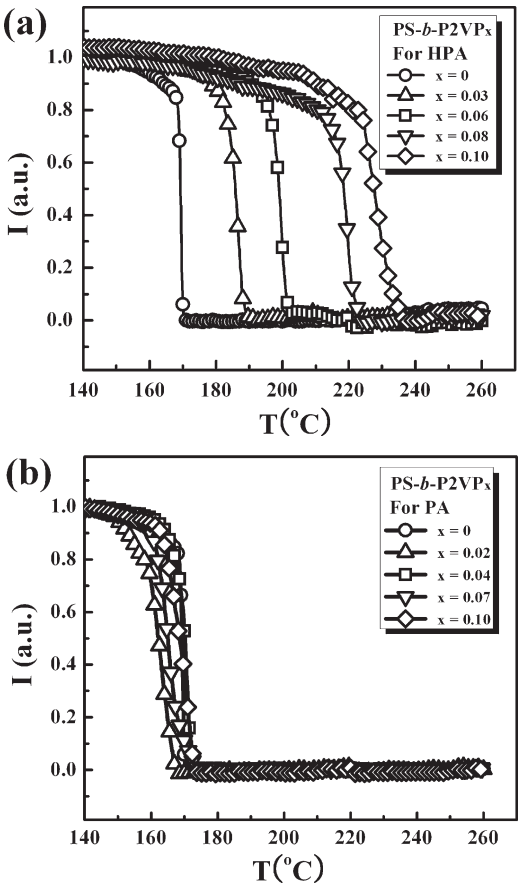


**Figure 4.** Depolarized light scattering (DPLS) intensity for BCP mixtures with (a) HPA and (b) PA as a function of temperature. All intensities were measured during heating process from 140 to 260 °C at a heating rate of 0.9 °C/min, and the maximum intensities were normalized to unity.

indicating an increase of $T_{ODT}$ by 69 °C compared to that for the pristine PS-*b*-P2VP. This increase represents the increase of nonfavorable segmental interactions ($\chi$) between two block components by the addition of HPA.

The scattering parameters derived from the SAXS profiles are plotted in Figure 3c as a function of inverse temperature (1/K). $T_{ODT}$ for BCP mixtures increases with increasing amount of HPA, which are determined by a discontinuous change in the inverse of the maximum intensity ($1/I(q^*)$), full width at half-maximum (fwhm), and *d*-spacing (d) by $d = 2\pi/q^*$. At higher temperatures than $T_{ODT}$, a remarkable increase in $1/I(q^*)$ and fwhm indicates that the thermal fluctuation increases proportionally to temperature since $\chi$ between two components decreases with increasing temperature. The *d*-spacing, as a characteristic length scale of the radius of gyration ($R_g$) for BCP mixtures, reveals a discontinuity at $T_{ODT}$ and gradually decreases with further increasing temperature. It also should be pointed out that an increase in *d*-spacing with increasing amount of HPA confirms the increase of nonfavorable segmental interactions between two block components rather than a volumetric increase.

To supplement transition information for BCP mixtures, the depolarized light scattering (DPLS) was used to probe the transition temperatures effectively due to the optical change between lamellar microdomains and isotropic disordered state of block copolymers. Figure 4a,b shows optical intensities for BCP mixtures as a function of temperature depending on the amount of HPA and PA, respectively. Such a high intensity at lower temperatures ($T < T_{ODT}$) for the pristine PS-*b*-P2VP arises from the optical anisotropy of the birefringent lamellar microdomains,

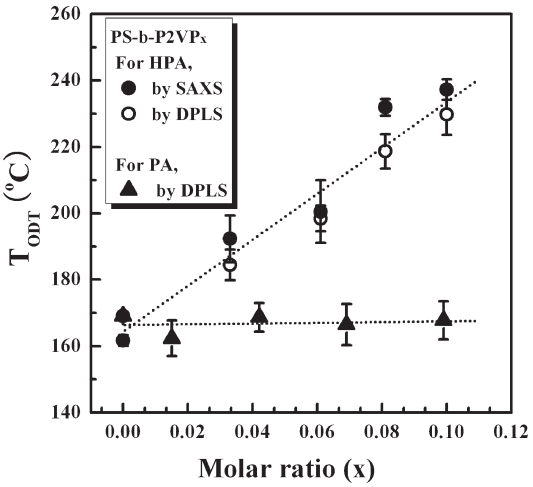


**Figure 5.** Transition temperatures (or $T_{ODT}$'s) evaluated by SAXS and DPLS measurements for BCP mixtures as a function of molar ratio (*x*) of HPA and PA to PS-*b*-P2VP. The dotted lines indicate the linear least-squares fits to $T_{ODT}$'s for BCP mixtures.

followed by a sharp decrease to zero at $T_{ODT}$ of $T$ = 167 °C, remaining disordered with further increasing temperature up to 260 °C due to the optical isotropy of phase-mixed state. Hence, transition temperatures can be confirmed by DPLS measurement taken by the discontinuity in intensity for BCP mixtures. An increase in $T_{ODT}$ with increasing amount of HPA is in good agreement with SAXS results within reasonable error range. A little difference in transitions between SAXS and DPLS measurements was observed because of the broad transitions or different mechanisms in temperature experiments. On the other hand, for BCP mixtures with PA in Figure 4b, there is no discernible change in the transition temperature with increasing amount of PA.

Figure 5 summarizes the transition temperatures (or $T_{ODT}$'s) evaluated by SAXS and DPLS measurements as a function of molar ratio (*x*) of HPA and PA to PS-*b*-P2VP. An increase in $T_{ODT}$ for BCP mixtures with increasing amount of HPA is in contrast to the similar $T_{ODT}$'s for BCP mixtures with PA. To further discuss whether HPA or PA locates in the specific block components in PS-*b*-P2VP, we investigated the phase miscibility (turbidity) between the monodisperse homopolymers and either HPA or PA. Turbidity measurement shows that HPA is miscible with P2VP homopolymers up to $M_n$ = 20 000 g/mol, but it turns out to be immiscible with PS homopolymers even when the molecular weight of PS is controlled down to $M_n$ = 7500 g/mol, which is close to the molecular weight for one component of PS-*b*-P2VP used in this study. However, PA is miscible with PS homopolymers up to $M_n$ = 24 000 g/mol but immiscible with P2VP homopolymers down to $M_n$ = 5000 g/mol. This molecular weight dependence on the phase miscibility leads to the fact that HPA favors P2VP component rather than PS component in PS-*b*-P2VP, while PA favors PS component. It should be here mentioned that WAXS (wide-angle X-ray scattering) and DSC results show no evidence for crystallization (or aggregation) of phenylacetamide derivatives in the mixtures. Therefore, Figure 5 in addition to the phase miscibility results enables us to speculate that the effective H-bonding between the nitrogen units of P2VP block and hydroxyl group in the HPA enhances nonfavorable segmental interactions between two block components during heating process because the difference in chemical structure between HPA and PA is only the hydroxyl functionality at phenylacetamide unit.

One may raise a key question whether the H-bonding at hydroxyl functionality is working at higher temperature than the melting temperature ($T_m$ = 178 °C) of HPA because the

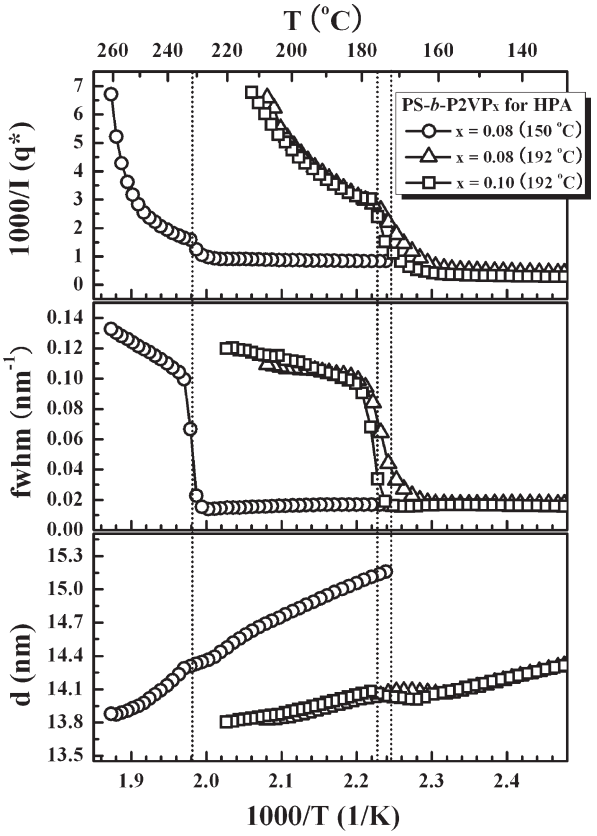


**Figure 6.** Annealing temperature dependence for BCP mixtures with HPA ($x$ = 0.08 and 0.10) between 150 and 192 °C, as measured with SAXS. The scattering parameters were derived from the SAXS profiles for BCP mixtures with HPA as a function of inverse temperature (1/K).

intermolecular interactions along with H-bonding weaken significantly above $T_m$ close to the dissociation temperature of H-bonding. To elucidate the influence of H-bonding on transition behavior, we set an annealing temperature to 192 °C for BCP mixtures with HPA at the same procedures. Figure 6 shows the scattering parameters derived from the SAXS profiles for BCP mixtures with HPA ($x$ = 0.08 and 0.10) as a function of inverse temperature (1/K), where the samples were annealed at 192 °C and compared to that annealed at 150 °C. A discontinuous change in the scattering parameters allows us to determine $T_{ODT}$ for BCP mixtures. For BCP mixtures with HPA of $x$ = 0.08 (and 0.10), transition temperatures for the samples annealed at 192 °C indicate $T_{ODT} \sim 170$ °C, which are much lower than that (232 °C) for the sample annealed at 150 °C. Even $d$-spacings at ordered state for the samples annealed at 192 °C are smaller than that for the sample annealed at 150 °C. The consistent results were confirmed by DPLS measurement, as shown in Figure 7 for BCP mixtures with HPA. Unlike an increase in $T_{ODT}$ with increasing amount of HPA up to $x$ = 0.10 for BCP mixtures annealed at 150 °C, the similar $T_{ODT}$'s (~170 °C) for BCP mixtures annealed at 192 °C were observed regardless of the amount of HPA. The differences in $T_{ODT}$ obtained from BCP mixtures annealed at different temperatures can be attributed to the availability of H-bonding depending on annealing temperatures, more than likely because the intermolecular interactions at 192 °C are so weak that BCP mixtures cannot form the effective H-bonding between the nitrogen units of P2VP block and hydroxyl group in the HPA, leading to the similar $T_{ODT}$'s. It should be noted that all the samples annealed at 140−170 °C, well below the melting temperature of HPA, indicate an increase in $T_{ODT}$ with increasing amount of HPA.

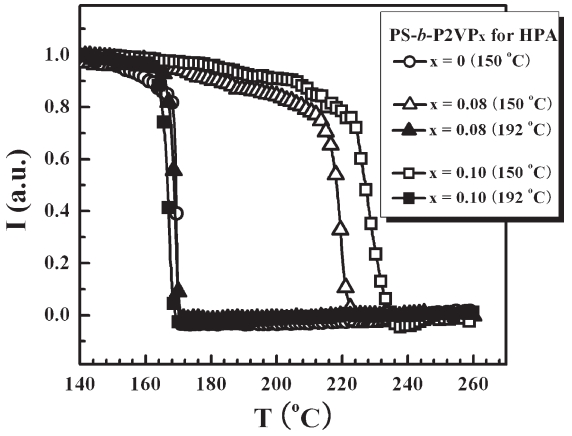


**Figure 7.** Annealing temperature dependence for BCP mixtures with HPA of $x$ = 0.08 and 0.10 between 150 and 192 °C, as measured with DPLS. All intensities were measured during heating process from 140 to 260 °C at a heating rate of 0.9 °C/min, and the maximum intensities were normalized to unity.

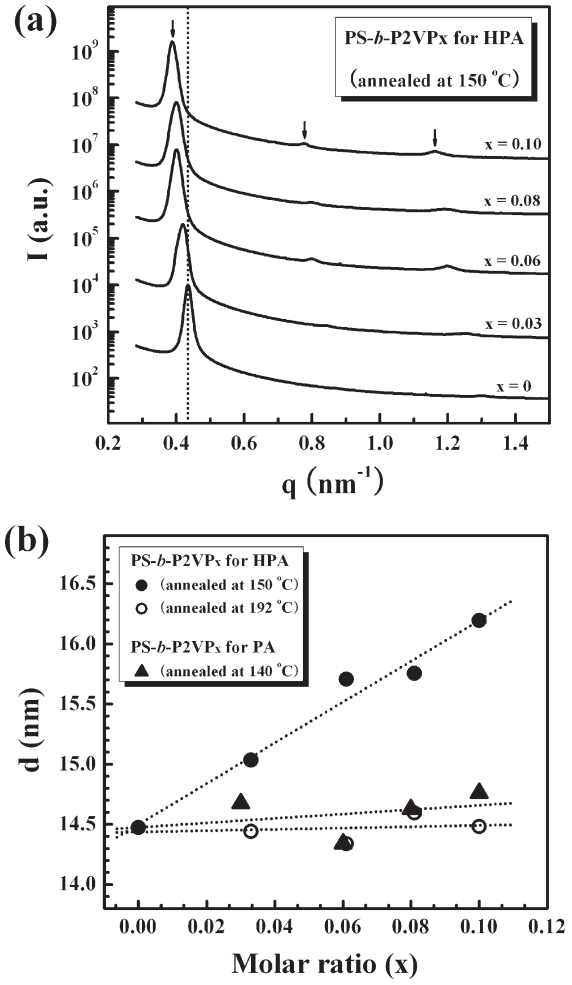


**Figure 8.** (a) SAXS intensity profiles for BCP mixtures with HPA, which were measured at room temperature after thermal annealing at 150 °C for 40 h. (b) $d$-spacing from the SAXS profiles for BCP mixtures as a function of molar ratio ($x$) of HPA and PA to PS-$b$-P2VP, which was measured at room temperature after thermal annealing at each temperature. The dotted lines indicate the linear least-squares fits to $d$-spacings for BCP mixtures.

Figure 8a shows SAXS intensity profiles for BCP mixtures with HPA, which were measured at room temperature after

thermal annealing at 150 °C for 40 h. The third-order peak for the pristine PS-*b*-P2VP with respect to the first-order reflection (or $q^*$) is weakly visible with no second-order peak presumably due to the volumetric symmetry between two block components. The development of the higher-order peaks (the peak ratios of $q/q^* = 1:2:3$) for BCP mixtures with HPA of $x = 0.10$ confirms the enhanced ordering degree of a typical lamellar morphology. Interestingly, the position of $q^*$ moves toward the lower $q$ as the amount of HPA increases up to $x = 0.10$, indicating an increase in *d*-spacing by addition of HPA. The *d*-spacing from the SAXS profiles measured at room temperature was analyzed as a function of molar ratio ($x$) of HPA and PA to PS-*b*-P2VP after thermal annealing at each temperature, as plotted in Figure 8b. For BCP mixtures with HPA, *d*-spacing for the samples annealed at 150 °C increases with increasing amount of HPA, whereas for the samples annealed at 192 °C, it remains relatively unchanged regardless of the amount of HPA, which is very similar to that for BCP mixtures with PA. The *d*-spacing, as a consequence of the thermodynamic balance between the domain free energy and interfacial energy of two block components, is proportional to $a(N^{2/3})(\chi^{1/6})$; $d \sim \chi^{1/6}$ in the strong segregation limit (SSL), where $a$ and $N$ are the statistical segmental length and the number of monomer, respectively.[41] Therefore, a variation of *d*-spacing represents the conformational changes of the polymer chains between two block components. Consequently, we can speculate that only the effective H-bonding between the nitrogen units of P2VP block and hydroxyl group in the HPA causes the block chains to stretch more in a direction perpendicular to the interfaces due to the increase of nonfavorable segmental interactions between two block components.

To ensure thermoreversibility for H-bonding, the sample annealed at 192 °C was reannealed at 150 °C for 3 days and an additiomal 10 days. Figure 9 shows FT-IR absorbance spectra for the pristine PS-*b*-P2VP and BCP mixtures with HPA of $x = 0.10$ depending on the annealing temperatures and times at selected wavenumber ($\nu$) range from 1800 to 1300 $cm^{-1}$. When the sample is annealed at 150 °C, two characteristic bands at 1675 and 1516 $cm^{-1}$ corresponding to C═O stretching and N−H deformation, respectively, indicate a concentration of HPA. Especially for the sample annealed at 192 °C, two characteristic bands disappear, presumably representing that these bands are generated by the effective H-bonding between the nitrogen units of P2VP block and hydroxyl group in the HPA, not by HPA only. Interestingly, the absorbance at two characteristic bands increases with increasing time when the sample was reannealed at 150 °C, although the maxima in absorbance were not recovered entirely. This indicates that a long time is necessary to recover H-bonding between a polymer chain and a low molecule.

On the basis of the results characterized by SAXS, DPLS, and FT-IR spectroscopy, we depict a schematic illustration in Figure 10 for BCP mixtures with HPA of $x = 0.10$ depending on the annealing temperatures. When the sample is annealed at 150 °C, BCP mixtures with HPA can form the effective H-bonding between the nitrogen units of P2VP block and hydroxyl group in the HPA, leading to a significant increase (12%) in *d*-spacing up to 16.2 nm, because the increase of nonfavorable segmental interactions between two block components causes the block chains to stretch more in a direction perpendicular to the interfaces. However, when the sample is annealed at 192 °C, the *d*-spacing for BCP mixtures with HPA indicates 14.5 nm, which is close to that for the BCP itself. This behavior describes that HPA detached from the nitrogen units and randomly displaced in P2VP block cannot influence transition behavior for PS-*b*-P2VP because of no meditation by H-bonding.

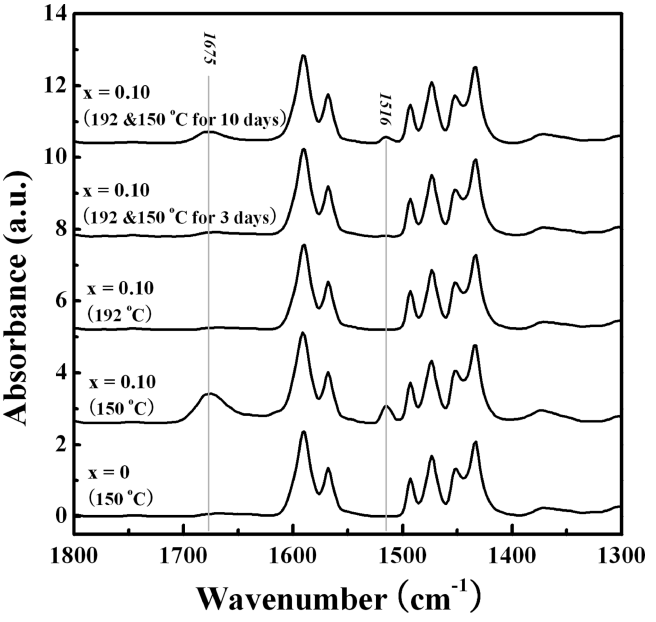


**Figure 9.** FT-IR absorbance spectra for BCP mixtures with HPA of $x = 0.10$ depending on the annealing temperatures between 150 and 192 °C and reannealing times for 3 and 10 days at 150 °C for the sample annealed at 192 °C. All the spectra were measured at room temperature.

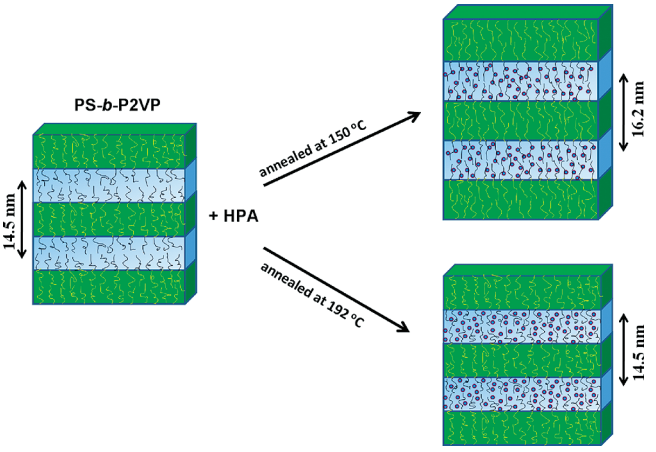


**Figure 10.** Schematic illustration for BCP mixtures with HPA of $x = 0.10$ depending on the annealing temperatures. For the samples annealed at 150 °C, a complex form by H-bonding between the nitrogen units of P2VP block and hydroxyl group in the HPA causes the block chains to stretch more in a direction perpendicular to the interfaces.

## Conclusion

Transition behavior for PS-*b*-P2VP mixtures with phenylacetamide derivatives such as HPA and PA was investigated to elucidate whether the H-bonding mediation efficiently influence transition temperatures, where an extra hydroxyl group in the HPA in comparison to PA is available for the intermolecular interactions with block copolymer. For BCP mixtures, we observed an increase in $T_{ODT}$ with increasing amount of HPA, while a similar $T_{ODT}$ regardless of the amount of PA. This indicates that the effective H-bonding between the nitrogen units of P2VP block and hydroxyl group in the HPA enhances nonfavorable segmental interactions between two block components during heating process, leading to a significant increase in *d*-spacing for BCP mixtures with HPA.

An annealing temperature dependence for BCP mixtures with HPA between 150 and 192 °C, measured by SAXS, DPLS, and

FT-IR, demonstrates that the sample annealed at 150 °C successfully forms the selective complex by H-bonding mediation between the nitrogen units of P2VP block and hydroxyl group in the HPA, while the sample annealed at 192 °C above the melting temperature ($T_m$ = 178 °C) of HPA leads to the lower transition temperature than that for the sample annealed at 150 °C. At higher temperatures (192 °C) than $T_m$ of HPA, the intermolecular interactions without H-bonding are so weak as to influence transition behavior for BCP mixtures although HPA is embedded in P2VP block component. In addition, a recovery for H-bonding mediation between a polymer chain (P2VP block) and HPA was observed when the sample is reannealed at 150 °C below $T_m$ of HPA, indicating a thermoreversibility for the molecular interactions. This result illustrates the importance of the availability for H-bonding mediation to control over transition behavior for BCP mixtures with the functional molecules.

**Acknowledgment.** This work was supported by the NRF grant (2009-0067295) and APCPI ERC program (R11-2007-050-00000) funded by the Ministry of Education, Science & Technology (MEST), Korea.

## References and Notes

(1) Jeong, B.; Bae, Y. H.; Lee, D. S.; Kim, S. W. *Nature* **1997**, *388* (6645), 860–862.
(2) Park, M.; Harrison, C.; Chaikin, P. M.; Register, R. A.; Adamson, D. H. *Science* **1997**, *276* (5317), 1401–1404.
(3) Discher, B. M.; Won, Y.-Y.; Ege, D. S.; Lee, J. C.-M.; Bates, F. S.; Discher, D. E.; Hammer, D. A. *Science* **1999**, *284* (5417), 1143–1146.
(4) Fasolka, M. J.; Mayes, A. M. *Annu. Rev. Mater. Res.* **2001**, *31* (1), 323–355.
(5) Jeong, B.; Kim, S. W.; Bae, Y. H. *Adv. Drug Delivery Rev.* **2002**, *54* (1), 37–51.
(6) Rapoport, N. *Prog. Polym. Sci.* **2007**, *32* (8−9), 962–990.
(7) Yang, S. Y.; Park, J.; Yoon, J.; Ree, M.; Jang, S. K.; Kim, J. K. *Adv. Funct. Mater.* **2008**, *18* (9), 1371–1377.
(8) Foerster, S.; Khandpur, A. K.; Zhao, J.; Bates, F. S.; Hamley, I. W.; Ryan, A. J.; Bras, W. *Macromolecules* **1994**, *27* (23), 6922–6935.
(9) Hajduk, D. A.; Harper, P. E.; Gruner, S. M.; Honeker, C. C.; Kim, G.; Thomas, E. L.; Fetters, L. J. *Macromolecules* **1994**, *27* (15), 4063–4075.
(10) Schulz, M. F.; Bates, F. S.; Almdal, K.; Mortensen, K. *Phys. Rev. Lett.* **1994**, *73*, 86.
(11) Khandpur, A. K.; Foerster, S.; Bates, F. S.; Hamley, I. W.; Ryan, A. J.; Bras, W.; Almdal, K.; Mortensen, K. *Macromolecules* **1995**, *28* (26), 8796–8806.
(12) Schulz, M. F.; Khandpur, A. K.; Bates, F. S.; Almdal, K.; Mortensen, K.; Hajduk, D. A.; Gruner, S. M. *Macromolecules* **1996**, *29* (8), 2857–2867.
(13) Zhao, J.; Majumdar, B.; Schulz, M. F.; Bates, F. S.; Almdal, K.; Mortensen, K.; Hajduk, D. A.; Gruner, S. M. *Macromolecules* **1996**, *29* (4), 1204–1215.
(14) Vigild, M. E.; Almdal, K.; Mortensen, K.; Hamley, I. W.; Fairclough, J. P. A.; Ryan, A. J. *Macromolecules* **1998**, *31* (17), 5702–5716.
(15) Ahn, J.-H.; Zin, W.-C. *Macromolecules* **2000**, *33* (2), 641–644.
(16) Zhu, L.; Huang, P.; Chen, W. Y.; Weng, X.; Cheng, S. Z. D.; Ge, Q.; Quirk, R. P.; Senador, T.; Shaw, M. T.; Thomas, E. L.; Lotz, B.; Hsiao, B. S.; Yeh, F.; Liu, L. *Macromolecules* **2003**, *36* (9), 3180–3188.
(17) Leibler, L. *Macromolecules* **1980**, *13* (6), 1602–1617.
(18) Bates, F. S.; Fredrickson, G. H. *Annu. Rev. Phys. Chem.* **1990**, *41* (1), 525–557.
(19) Hashimoto, T. *Thermoplastic Elastomers*; Hanser: New York, 1996.
(20) Bates, F. S.; Rosedale, J. H.; Bair, H. E.; Russell, T. P. *Macromolecules* **1989**, *22* (6), 2557–2564.
(21) Rosedale, J. H.; Bates, F. S. *Macromolecules* **1990**, *23* (8), 2329–2338.
(22) Bondzic, S.; de Wit, J.; Polushkin, E.; Schouten, A. J.; ten Brinke, G.; Ruokolainen, J.; Ikkala, O.; Dolbnya, I.; Bras, W. *Macromolecules* **2004**, *37* (25), 9517–9524.
(23) Pollino, J. M.; Weck, M. *Chem. Soc. Rev.* **2005**, *34* (3), 193–207.
(24) Ruokolainen, J.; Mäkinen, R.; Torkkeli, M.; Mäkelä, T.; Serimaa, R.; ten Brinke, G.; Ikkala, O. *Science* **1998**, *280* (5363), 557–560.
(25) Tung, S.-H.; Kalarickal, N. C.; Mays, J. W.; Xu, T. *Macromolecules* **2008**, *41* (17), 6453–6462.
(26) Zhang, H.; Fu, Y.; Wang, D.; Wang, L.; Wang, Z.; Zhang, X. *Langmuir* **2003**, *19* (20), 8497–8502.
(27) Valkama, S.; Ruotsalainen, T.; Nykanen, A.; Laiho, A.; Kosonen, H.; ten Brinke, G.; Ikkala, O.; Ruokolainen, J. *Macromolecules* **2006**, *39* (26), 9327–9336.
(28) Ruokolainen, J.; Torkkeli, M.; Serimaa, R.; Komanschek, E.; ten Brinke, G.; Ikkala, O. *Macromolecules* **1997**, *30* (7), 2002–2007.
(29) de Wit, J.; van Ekenstein, G. A.; Polushkin, E.; Kvashnina, K.; Bras, W.; Ikkala, O.; ten Brinke, G. *Macromolecules* **2008**, *41* (12), 4200–4204.
(30) Ikkala, O.; ten Brinke, G. *Science* **2002**, *295* (5564), 2407–2409.
(31) Lehn, J.-M. *Chemistry. Concepts and Perspectives*; Wiley-VCH: New York, 1995.
(32) Lee, D. H.; Han, S. H.; Joo, W.; Kim, J. K.; Huh, J. *Macromolecules* **2008**, *41* (7), 2577–2583.
(33) Ribbe, A. E.; Okumura, A.; Matsushige, K.; Hashimoto, T. *Macromolecules* **2001**, *34* (23), 8239–8245.
(34) Ruokolainen, J.; Eerikainen, H.; Torkkeli, M.; Serimaa, R.; Jussila, M.; Ikkala, O. *Macromolecules* **2000**, *33* (25), 9272–9276.
(35) Ruokolainen, J.; Torkkeli, M.; Serimaa, R.; Vahvaselka, S.; Saariaho, M.; ten Brinke, G.; Ikkala, O. *Macromolecules* **1996**, *29* (20), 6621–6628.
(36) Tung, S.-H.; Xu, T. *Macromolecules* **2009**, *42* (15), 5761–5765.
(37) Shibata, M.; Kimura, Y.; Yaginuma, D. *Polymer* **2004**, *45* (22), 7571–7577.
(38) Xiao, S.; Lu, X.; Lu, Q.; Su, B. *Macromolecules* **2008**, *41* (11), 3884–3892.
(39) Kim, B.; Ahn, H.; Kim, J. H.; Ryu, D. Y.; Kim, J. *Polymer* **2009**, *50* (15), 3822–3827.
(40) Young, W.-S.; Epps, T. H. *Macromolecules* **2009**, *42* (7), 2672–2678.
(41) Matsen, M. W.; Bates, F. S. *Macromolecules* **1996**, *29* (4), 1091–1098.